General Relativistic Models of Binary Neutron Stars in Quasiequilibrium

T. W. Baumgarte
Department of Physics, University of Illinois at Urbana-Champaign, Urbana, Il 61801

G. B. Cook, M. A. Scheel
Center for Radiophysics and Space Research, Cornell University, Ithaca, NY 14853

S. L. Shapiro
Departments of Physics and Astronomy and National Center for Supercomputing Applications, University of Illinois at Urbana-Champaign, Urbana, Il 61801

S. A. Teukolsky
Departments of Physics and Astronomy and Center for Radiophysics and Space Research, Cornell University, Ithaca, NY 14853

We perform fully relativistic calculations of binary neutron stars in corotating, circular orbit. While Newtonian gravity allows for a strict equilibrium, a relativistic binary system emits gravitational radiation, causing the system to lose energy and slowly spiral inwards. However, since inspiral occurs on a time scale much longer than the orbital period, we can treat the binary to be in quasiequilibrium. In this approximation, we integrate a subset of the Einstein equations coupled to the relativistic equation of hydrostatic equilibrium to solve the initial value problem for binaries of arbitrary separation. We adopt a polytropic equation of state to determine the structure and maximum mass of neutron stars in close binaries for polytropic indices $n = 1$, 1.5 and 2. We construct sequences of constant rest-mass and locate turning points along energy equilibrium curves to identify the onset of orbital instability. In particular, we locate the innermost stable circular orbit (ISCO) and its angular velocity. We construct the first contact binary systems in full general relativity. These arise whenever the equation of state is sufficiently soft ($n \gtrsim 1.5$). A radial stability analysis reveals no tendency for neutron stars in close binaries to collapse to black holes prior to merger.

PACS numbers: 04.20.Ex, 04.25.Dm, 04.30.Db, 04.40.Dg, 97.60.Jd

I. INTRODUCTION

Neutron star binaries are interesting for numerous reasons. Several neutron star binary systems are known to exist even within our own galaxy [1]. For some of these systems (including PSR B1913+16, B1534+12) general relativistic effects in the binary orbit have been measured to high precision [2,3]. Binary neutron stars are believed to be among the most promising sources of gravitational waves for detectors like LIGO, VIRGO and GEO. This circumstance has triggered multiple efforts to predict the gravitational waveform emitted during the inspiral and the final plunge of the two stars. More fundamentally, the two-body problem is one of the outstanding unsolved problems in classical general relativity.

Considerable effort has gone into understanding binary neutron stars. Most of this work has been performed within the framework of Newtonian hydrodynamics. Hachisu and Eriguchi [4] constructed hydrostatic equilibrium of binaries in synchronized circular orbits. Rasio and Shapiro [5] studied binary equilibrium configurations and their dynamical evolution, including the merger of the two stars. The coalescence of neutron star binaries has also been investigated by Shibata, Nakamura and Oohara [6], Zhuge, Centrella and McMillan [7] and Ruffert, Janka and Schäfer [8] and other investigators.

Many investigators have also studied the binary problem within a post-Newtonian framework. As long as the stars are well separated they can be approximated by point sources. In this case hydrodynamical effects are neglected and the gravitational waveform can be calculated to second post-Newtonian order (see [9] and references therein). Post-Newtonian calculations that do take into account hydrodynamical effects are also under way: Shibata [10] and Taniguchi and Shibata [11] have constructed equilibrium configurations and Oohara and Nakamura [12] have studied binary coalescence. Lai [13], Lai and Wiseman [14] and Lombardi, Rasio and Shapiro [15] have constructed binary equilibrium configurations in an ellipsoidal approximation.

Fully general relativistic treatments of the problem are complicated by several factors, including the nonlinearity of the partial differential equations and the requirement of very large computational resources to solve the coupled system. These simulations are currently only in their infancy [12]. Recently, Wilson, Mathews and Marronetti [16] (hereafter WMM) reported results obtained with a relativistic numerical code. Their

code assumed several simplifying physical and mathematical approximations. Their results suggest that the central densities of the stars increase as the stars approach each other and that massive neutron stars individually collapse to black holes prior to merger. WMM therefore find that in general relativity, the presence of a companion star and its tidal field tend to destabilize the stars in a binary system. This conclusion is opposite to what is expected from Newtonian [17], post-Newtonian [13–15,18], perturbative [19] and matched asymptotic expansion [20,21] treatments of the problem. WMM also find that just prior to plunge and merger, their binary system has a total angular momentum too large to form a Kerr black hole (see the discussion in [22]).

In this paper we construct fully relativistic binary neutron stars in quasiequilibrium circular orbit ("quasi"-equilibrium because these binaries are not strictly stationary: because of the slow emission of gravitational radiation, general relativistic binaries cannot be in strict equilibrium). These models are interesting on their own right and provide initial data for future dynamical evolution calculations. We study the structure of the neutron stars in these close binary systems and determine, for example, their maximum allowed equilibrium mass. In addition, we build quasiequilibrium binary sequences of constant rest-mass. These sequences approximate evolutionary trajectories of neutron star binaries undergoing slow inspiral via the generation of gravitational radiation. By locating the turning points in their total energy versus separation curves, we can identify the onset of orbital instability at the innermost stable circular orbit (ISCO) and the orbital parameters at that critical radius. We have presented preliminary results in [23], and analyzed the stability of these binaries in [24]. We do not find any evidence for a destabilization of neutron stars in close binaries.

The purpose of this paper is to discuss details of our approximations, equations, and numerical method, and to present more complete results. The paper is organized as follows: in Section II we discuss all the underlying assumptions and approximations made in our calculations. In Section III we derive all the equations describing the quasiequilibrium of relativistic binary neutron stars. The numerical implementation of these equations is described in Section IV. We present results for several different polytropic equations of state in Section V and briefly summarize our findings in Section VI. We also include an Appendix with tabulated data for some of our sequences.

II. BASIC ASSUMPTIONS AND APPROXIMATIONS

Throughout this paper we will assume that the two neutron stars have equal mass, are corotating in a circular orbit and that the matter obeys a polytropic equation of state.

Choosing a polytropic equation of state permits a wide survey of models as a function of the stiffness of the equation of state and also simplifies the integration of the matter equation (33). However, polytropic equations could be easily replaced by more realistic cold equations of state.

Restricting our analysis to stars with equal masses allows us to exploit spatial symmetry and solve the problem in just one octant in our Cartesian grid (see Section III A below). However, generalizing our method to stars of unequal mass is straightforward. Nevertheless, it is interesting to note that all well determined masses of neutron stars in close binary systems have masses remarkably close to $1.4M_\odot$ (see, for example, [1]). Focussing on stars with equal mass may therefore be physically reasonable as well as numerically convenient.

Demanding that the stars be corotating is a much less realistic assumption. Even if the stars in a binary started out corotating at a large separation, maintaining this corotation during inspiral would require a larger viscosity than is possible in neutron stars [25,26]. Instead, it is more likely that the circulation of the stars is conserved during inspiral. However, our assumption of corotation greatly simplifies the solution of the problem (see Section III B) and it is appropriate to tackle this simpler case first. Even in Newtonian theory, the construction of nonsynchronous binaries is difficult because of the unknown velocity field; only in ellipsoidal models can one build nonsynchronous as easily as synchronous binaries [15]. Constructing more realistic sequences of constant circulation requires a dynamical treatment, as one marches inward from one radius to the next using the full coupled set of field and hydrodynamic evolution equations to guarantee conservation of circulation.

In Newtonian gravity, a strict equilibrium solution for two such stars in a synchronized circular orbit always exists, except for very stiff equations of state (with $n \lesssim 1.5$) near contact [4]. Since this solution is stationary, the hydrodynamical equations for the matter reduce to a single Bernoulli integral, which greatly simplifies the problem (see Section III C).

Because of the emission of gravitational waves, a binary in general relativity cannot be in strict equilibrium. However, up to the innermost stable circular orbit (ISCO), the timescale for orbital decay by radiation will be much longer than the orbital period, so that the binary can be considered to be in "quasiequilibrium". This allows us to neglect both gravitational waves and wave-induced deviations from a circular orbit to good approximation. A similar approximation is often used in stellar evolution calculations: there the relevant evolution timescales are the nuclear or Kelvin-Helmholtz timescales, while the stars maintain (quasi) hydrostatic equilibrium on a dynamical timescale.

We attempt to minimize the gravitational wave content by choosing the spatial metric to be conformally flat, as in WMM (see also [27]). As will be shown in

Section III A, the field equations then reduce to a set of coupled, quasi-linear elliptic equations for the lapse, the shift and the conformal factor. If we neglect small deviations from circular orbit, the fluid flow is again stationary, and the hydrodynamical equations again reduce to a relativistic Bernoulli integral (see Section III B). Solving these equations yields a valid solution to the initial value (constraint) equations, and an approximate solution to the full Einstein equations for an inspiraling binary at any given moment, prior to plunge.

This conformal approximation has been carefully tested in Ref. [28] for a single rotating star in stationary equilibrium, which is the simplest numerical example in relativity for which the equilibrium solution deviates from conformal flatness. In Ref. [28] it was shown that by assuming conformal flatness, the resulting deviations from the exact solution were typically much smaller than 1%, even for highly relativistic stars.

III. BASIC EQUATIONS

A. Field Equations

To construct a numerical model of a binary system we employ the ADM decomposition of Einstein's equations of general relativity [29]. The derivation of our adopted equations closely follows the derivation in [28] for rotating stars.

We write the metric in the general form

$$ds^2 = -\alpha^2 dt^2 + \gamma_{ij}(dx^i - \omega^i dt)(dx^j - \omega^j dt). \quad (1)$$

Throughout the paper Latin indices will run from 1 to 3, whereas Greek indices will run from 0 to 3. We also set $G = c = 1$. By definition of the extrinsic curvature K_{ij}, the three-metric γ_{ij} satisfies the dynamical equation

$$\partial_t \gamma_{ij} = -2\alpha K_{ij} - D_i\omega_j - D_j\omega_i, \quad (2)$$

where D_i denotes the covariant derivative associated with γ_{ij}. This equation can be decomposed into its trace

$$\partial_t \ln \gamma^{1/2} = -\alpha K - D_i\omega^i, \quad (3)$$

where $\gamma = \det \gamma_{ij}$ and $K = K^i{}_i$, and its trace-free part

$$\gamma^{1/3}\partial_t(\gamma^{-1/3}\gamma_{ij}) = -2\alpha(K_{ij} - \frac{1}{3}\gamma_{ij}K) - D_i\omega_j - D_j\omega_i + \frac{2}{3}\gamma_{ij}D_k\omega_k. \quad (4)$$

In the following we will choose maximal slicing so that

$$K = 0. \quad (5)$$

We expect the gravitational wave content of the spacetime to be small (see Section II), and we now want to use this expectation to simplify the problem. Unfortunately, the physical fields cannot be cleanly separated into freely specifiable dynamical degrees of freedom and dependent quantities, which are determined by the constraint equations. However, such an identification is possible with the help of a conformal decomposition [30]. We can therefore attempt to minimize the gravitational wave content of the (physical) spacetime by removing the dynamical (or "wave") degrees of freedom from the conformal fields. This can be achieved by choosing the three-metric γ_{ij} to be conformally flat, so that $\gamma^{-1/3}\gamma_{ij} = f_{ij}$, where f_{ij} is the flat space metric. We will later use Cartesian coordinates, for which f_{ij} becomes the Kronecker delta δ_{ij}. Note that this choice can always be made to find initial data on one time slice without any approximation. Our approximation lies in assuming that the metric will *remain* conformally flat for all times during the inspiral. Eq. (4) then reduces to [31]

$$2\alpha K_{ij} = -D_i\omega_j - D_j\omega_i + \frac{2}{3}\gamma_{ij}D_k\omega^k. \quad (6)$$

We now write the metric as

$$\gamma_{ij} = \Psi^4 f_{ij}, \quad (7)$$

where Ψ is the conformal factor. The later is determined by the Hamiltonian constraint

$$R - K_{ij}K^{ij} = 16\pi\rho, \quad (8)$$

where the source term ρ is defined by

$$\rho = n^\alpha n^\beta T_{\alpha\beta}. \quad (9)$$

Here n^α is the normal vector to a $t = $ const slice and $T_{\alpha\beta}$ is the stress-energy tensor. For the metric (7), the Ricci scalar R in (8) reduces to

$$R = -8\Psi^{-5}\nabla^2\Psi, \quad (10)$$

where ∇^2 is the flat space Laplacian associated with f_{ij}. Inserting this into (8) we find

$$\nabla^2\Psi = -\frac{1}{8}\Psi^{-7}\tilde{K}_{ij}\tilde{K}^{ij} - 2\pi\Psi^5\rho. \quad (11)$$

Here we have transformed K^{ij} according to

$$\tilde{K}^{ij} = \Psi^{10}K^{ij}, \quad (12)$$

which, from Eq. (6), now satisfies

$$\tilde{K}^{ij} = -\frac{\Psi^6}{2\alpha}\left(\nabla^i\omega^j + \nabla^j\omega^i - \frac{2}{3}f^{ij}\nabla_k\omega^k\right). \quad (13)$$

Inserting this expression into the momentum constraint

$$D_jK^{ij} = 8\pi j^i \quad (14)$$

yields

$$\nabla^2\omega^i + \frac{1}{3}\nabla^i(\nabla_j\omega^j) = 2\nabla_j \ln(\alpha\Psi^{-6})\tilde{K}^{ij} - 16\pi\alpha\Psi^4 j^i. \tag{15}$$

Here the source term j^i is given by

$$j^\alpha = -\gamma^\alpha{}_\beta n_\gamma T^{\beta\gamma}. \tag{16}$$

This equation can be simplified by writing the shift vector as a sum of a vector and a gradient [32]

$$\omega^i = G^i - \frac{1}{4}\nabla^i B. \tag{17}$$

Eq. (15) can then be replaced by the two equations

$$\nabla^2 G^i = 2\nabla_j \ln(\alpha\Psi^{-6})\tilde{K}^{ij} - 16\pi\alpha\Psi^4 j^i \tag{18}$$

and

$$\nabla^2 B = \nabla_i G^i. \tag{19}$$

Imposing the full set of dynamical equations for the evolution of K_{ij} would be inconsistent with Eq. (6) and our approximation that γ_{ij} remains conformally flat at all times. However, in addition to Eq. (5) we can always require that the maximal slicing condition be preserved $\partial_t K = 0$. Taking the trace of the time evolution equation for K_{ij} together with Eq. (11) then yields an equation for the lapse

$$\nabla^2(\alpha\Psi) = \alpha\Psi\left(\frac{7}{8}\Psi^{-8}\tilde{K}_{ij}\tilde{K}^{ij} + 2\pi\Psi^4(\rho + S)\right). \tag{20}$$

Here the source term S is defined by

$$S = \gamma^{ij}T_{ij}. \tag{21}$$

Eqs. (11), (18), (19) and (20) together with the matter equations (see next Section) form a system of coupled, nonlinear elliptic equations, which has to be solved iteratively. The boundary conditions follow from asymptotic flatness. Following Bowen [33], the exterior solution to the field equations can be expanded in terms of multipole moments. We adopt as outer boundary conditions the fall-off behavior of the lowest order non-vanishing multipole moments. Because of the symmetries of the problem it is possible to solve it in only one octant of a Cartesian grid. The resulting boundary conditions on the coordinate planes together with the outer boundary conditions are summarized in Table 1.

$r \to \infty$	$x = 0$	$y = 0$	$z = 0$
$G^x \sim \frac{z}{r^3}$	$\partial_x G^x = 0$	$\partial_y G^x = 0$	$G^x = 0$
$G^y \sim \frac{xyz}{r^7}$	$G^y = 0$	$G^y = 0$	$G^y = 0$
$G^z \sim \frac{x}{r^3}$	$G^z = 0$	$\partial_y G^z = 0$	$\partial_z G^z = 0$
$B \sim \frac{xz}{r^3}$	$B = 0$	$\partial_y B = 0$	$B = 0$
$\alpha - 1 \sim \frac{1}{r}$	$\partial_x \alpha = 0$	$\partial_y \alpha = 0$	$\partial_z \alpha = 0$
$\Psi - 1 \sim \frac{1}{r}$	$\partial_x \Psi = 0$	$\partial_y \Psi = 0$	$\partial_z \Psi = 0$

TABLE I. Boundary conditions for the outer boundaries ($r \to \infty$) and on the coordinate planes in Cartesian coordinates. The equatorial plane is taken to be the $y = 0$ plane and the stars are taken to be aligned with the z-axis.

B. Matter Equations

As we have discussed in Section II, we neglect wave-induced deviations from a strictly periodic, circular orbit, and also assume the stars to be corotating. In Cartesian coordinates we can choose the equatorial plane to be the $y = 0$ plane, so that the fluid four velocity then takes the form

$$u^\alpha = u^t(1, \Omega z, 0, -\Omega x), \tag{22}$$

where Ω is the constant angular velocity. We introduce a vector

$$\xi^\alpha = (0, z, 0, -x), \tag{23}$$

in terms of which the four velocity can also be written

$$u^\alpha = u^t(\alpha n^\alpha + \Omega\xi^\alpha - \omega^\alpha). \tag{24}$$

Define v to be the relative velocity between the matter and a normal observer

$$\frac{1}{(1-v^2)^{1/2}} = -n_\alpha u^\alpha = \alpha u^t. \tag{25}$$

Then, from $u^\alpha u_\alpha = -1$, we find

$$v^2 = \frac{\Psi^4}{\alpha^2}\left((\Omega z - \omega^x)^2 + (\omega^y)^2 + (\Omega x + \omega^z)^2\right). \tag{26}$$

For a perfect fluid the stress energy tensor is

$$T^{\alpha\beta} = (\rho_0 + \rho_i + P)u^\alpha u^\beta + P g^{\alpha\beta}, \tag{27}$$

where ρ_0 is the rest-mass density, ρ_i is the internal energy density and P is the pressure. The source term ρ in Eq. (9) can then be written

$$\rho = \frac{\rho_0 + \rho_i + P}{1 - v^2} - P, \tag{28}$$

the momentum source j^i in Eq. (16) becomes

$$j^i = \frac{(\rho_0 + \rho_i + P)}{\alpha}\frac{(\Omega\xi^i - \omega^i)}{1 - v^2}, \tag{29}$$

and S in Eq. (21) is given by

$$S = (\rho_0 + \rho_i + P)\frac{v^2}{1-v^2} + 3P. \tag{30}$$

In order to describe the matter close to equilibrium we will use two of our basic assumptions. Neglecting deviations from a strictly periodic circular orbit and taking the two stars to be corotating is equivalent to assuming that the fluid four velocity is proportional to a Killing vector

$$\frac{\partial}{\partial t} + \Omega\frac{\partial}{\partial \phi}. \tag{31}$$

In this approximation, the matter equations can be integrated analytically, which yields the relativistic Bernoulli integral (see, e.g., [34])

$$\frac{u^t}{h} = \text{const.} \tag{32}$$

Here h is the enthalpy

$$h = \exp\left(\int \frac{dP}{\rho_0 + \rho_i + P}\right). \tag{33}$$

For a polytropic equation of state

$$P = \kappa\rho_0^{1+1/n}, \tag{34}$$

where κ is the polytropic constant and n the polytropic index, the enthalpy becomes

$$h = \frac{\rho_0 + \rho_i + P}{\rho_0}. \tag{35}$$

It is very useful to introduce a dimensionless ratio

$$q = \frac{P}{\rho_0}, \tag{36}$$

in terms of which we can express

$$\rho_0 = \kappa^{-n} q^n \tag{37}$$

$$\rho_i = n\kappa^{-n} q^{n+1} \tag{38}$$

$$P = \kappa^{-n} q^{n+1}. \tag{39}$$

Note that in the Newtonian limit we have $q \ll 1$. Inserting the last three expressions together with Eqs. (25) and (35) into Eq. (32) we find

$$q = \frac{1}{1+n}\left(\frac{1+C}{\alpha(1-v^2)^{1/2}} - 1\right), \tag{40}$$

where we have written the constant in Eq. (32) as $1 + C$. Also, we use q to rewrite the source terms (28–30) as

$$\rho = \kappa^{-n} q^n \left(\frac{1+(1+n)q}{1-v^2} - q\right) \tag{41}$$

$$j^i = \kappa^{-n} q^n \frac{(1+(1+n)q)}{\alpha}\frac{(\Omega\xi^i - \omega^i)}{1-v^2} \tag{42}$$

$$\rho + 2S = \kappa^{-n} q^n \left(\frac{1+(1+n)q}{1-v^2}(1+2v^2) + 5q\right). \tag{43}$$

Note that physical dimensions enter our problem only through the polytropic constant κ in the equation of state (34). It is therefore useful to nondimensionalize all equations and eliminate κ from the problem. This means that given the polytropic index n, we can solve the equations once and use the results for arbitrary κ. Since $\kappa^{n/2}$ has units of length we can introduce dimensionless coordinates $\bar{t} = \kappa^{-n/2}t$, $\bar{x} = \kappa^{-n/2}x$ and the same for y and z. The derivative operator scales as $\bar{\nabla}_i = \kappa^{n/2}\nabla_i$, and the extrinsic curvature as $\bar{K}^{ij} = \kappa^{n/2}\tilde{K}^{ij}$. The angular velocity Ω transforms according to $\bar{\Omega} = \kappa^{n/2}\Omega$. We also rescale $\bar{B} = \kappa^{-n/2}B$ and $\bar{\xi}^i = \kappa^{-n/2}\xi^i$ Putting terms together we find the Hamiltonian constraint

$$\bar{\nabla}^2\Psi = -\frac{1}{8}\Psi^{-7}\bar{K}_{ij}\bar{K}^{ij} - 2\pi\Psi^5 q^n\left(\frac{1+(1+n)q}{1-v^2} - q\right), \tag{44}$$

the lapse equation

$$\bar{\nabla}^2\tilde{\alpha} = \tilde{\alpha}\frac{7}{8}\Psi^{-8}\bar{K}_{ij}\bar{K}^{ij} + 2\pi\tilde{\alpha}\Psi^4 q^n\left((1+(n+1)q)\frac{1+2v^2}{1-v^2} + 5q\right), \tag{45}$$

and the momentum constraint equations

$$\bar{\nabla}^2 G^i = -2\bar{\nabla}_j(\tilde{\alpha}\Psi^{-7})\bar{K}^{ij} - 16\pi\Psi^4 q^n\frac{1+(1+n)q}{1-v^2}(\bar{\Omega}\bar{\xi}^i - \omega^i) \tag{46}$$

and

$$\bar{\nabla}^2\bar{B} = \bar{\nabla}_i G^i. \tag{47}$$

Here we have used

$$\tilde{\alpha} = \Psi\alpha. \tag{48}$$

Eqs. (44–47) together with (40) form a set of seven equations for the seven unknowns Ψ, α, G^i, $\bar{B}$ and q. More specifically, we have to find a solution to six coupled, quasi-linear elliptic equation for the gravitational fields, together with one algebraic equation for the matter. $\bar{K}^{ij}$ and ω^i in the above expressions can be expressed in terms of the unknowns with the help of Eqs. (13) and (17).

C. The Newtonian Limit

In this Section we will briefly show that in the Newtonian limit the above equations approach the expected form. In particular we expect

$$\alpha \to e^{\Phi} \sim 1 + \Phi, \tag{49}$$

where Φ is the Newtonian potential. Also, in the Newtonian limit $\Phi, C, v \ll 1$, so that (40) becomes

$$\begin{aligned} q &= \frac{1}{n+1}\left(C - \Phi + \frac{1}{2}v^2\right) \\ &= \frac{1}{n+1}\left(C - \Phi + \frac{1}{2}\Omega^2(x^2+z^2)\right). \end{aligned} \tag{50}$$

Here we have used $\omega^i = 0$ (absence of frame dragging in the Newtonian limit). This limit, by Eq. (13), implies $K^{ij} = 0$. With $q \ll 1$, Eq. (44) now reduces to

$$\nabla^2 \Psi = -2\pi \Psi^5 q^n. \tag{51}$$

Identifying

$$\Psi \to e^{-\Phi/2} \sim 1 - \frac{\Phi}{2} \tag{52}$$

yields, to leading order, the Poisson equation

$$\nabla^2 \Phi = 4\pi\rho_0. \tag{53}$$

Eq. (45) gives the same limit.

IV. NUMERICAL METHOD

A. Constructing Quasiequilibrium Models

Corotating, equal mass binaries in circular orbits form a two-parameter family (just like single, uniformly rotating stars). A particular configuration is uniquely determined by two independent parameters. For computational purposes it is particularly convenient to choose these parameters to be the maximum density $q_{\max}$ and the relative separation of the stars [35].

As mentioned in Section III, we choose the stars to orbit in the $y = 0$ plane and to be aligned with the z-axis. In this case the surface of one star will intersect the z-axis at two different places. We will label the intersection closer to the origin of the coordinate system $\bar{r}_A$ and the one further out $\bar{r}_B$. The ratio

$$z_A \equiv \bar{r}_A / \bar{r}_B \tag{54}$$

then parametrizes the relative separation of the stars. We can construct an algorithm for solving the gravitational and matter equations by modifying the algorithm used by several authors for single rotating stars [47,37,38]. Making this algorithm stable requires rescaling the coordinates with respect to $\bar{r}_B$ so that

$$\hat{x} = \bar{x}/\bar{r}_B \qquad \hat{y} = \bar{y}/\bar{r}_B \qquad \hat{z} = \bar{z}/\bar{r}_B, \tag{55}$$

which means that the outer edge of the matter will always be at $\hat{r}_B = 1$. We also rescale

$$\hat{K}_{ij} = \bar{K}_{ij}\bar{r}_B \qquad \hat{B} = \bar{B}/\bar{r}_B \qquad \hat{\Omega} = \bar{\Omega}\bar{r}_B. \tag{56}$$

Eqs. (40) and (44–47) are left unchanged, except that the matter source terms in (44–46) have to be multiplied by $\bar{r}_B^2$ and $\bar{\nabla}_i$ has to be replaced by $\hat{\nabla}_i$. This rescaling then allows us to determine $\bar{r}_B$ as well as the the angular velocity $\hat{\Omega}$ and the matter constant C via an iteration process that uses q_{max} and z_A as the two input parameters.

The iteration scheme starts with an initial guess for the rest density distribution. We chose the density profile of an isolated, spherical star, i.e. we integrate the Tolman-Oppenheimer-Volkoff equations for the central density $q_{\max}$ and rescale the profile such that it fits between $\hat{r}_A = z_A$ and $\hat{r}_B = 1$. For this matter distribution we can then find a solution to the field equations (44–47) using a full approximation storage multigrid scheme (see, e.g., [39]).

Once a solution to the field equations has converged to an adequate accuracy on the finest level of the grid hierarchy, we evaluate Eq. (40) at three different locations to find new values for the constants $\hat{\Omega}$, C and $\bar{r}_B$ as well as a new density distribution. To do so we first search for the maximum density along the z-axis [40] and call this location $\hat{r}_C$. We can then evaluate Eq. (40) at the three points $\hat{r}_A$, $\hat{r}_B$ and $\hat{r}_C$

$$(1 + (n+1)q)\left(\alpha^2 - \Psi^4(\hat{\Omega}\hat{z} - w^x)^2\right)^{1/2} = 1 + C, \tag{57}$$

where we have used $x = y = \omega^y = \omega^z = 0$ on the z-axis. Note that at $\hat{r}_A$ and $\hat{r}_B$ the density vanishes $q = 0$. This set, on first sight, looks like three equations for the two unknows Ω and C. However, changing the scaling parameter $\bar{r}_B$ will also change the gravitational fields, so that α and Ψ will implicitly depend on $\bar{r}_B$. We determine how α and Ψ scale from the Newtonian limit. Rescaling the Poisson equation shows that the Newtonian potential Φ scales with $\bar{r}_B^2$. Eqs. (49) and (52) therefore suggest that α and Ψ should be rescaled according to

$$\alpha = (\hat{\alpha})^{\bar{r}_B^2} \qquad \Psi = (\hat{\Psi})^{-\bar{r}_B^2/2}. \tag{58}$$

Inserting these scale relations into (57) then yields three equations for the three constants $\hat{\Omega}$, C and $\bar{r}_B$, which can be solved iteratively. Once the constants have been determined the new matter distribution can be calculated using Eq. (40).

The iteration can then be continued by finding the new fields for the new matter distribution. At each step we calculate the residuals of Eqs. (44–47) and integrate these over the numerical grid. We typically stop the iteration when the sum of these six integrated residuals is smaller than about 1 % of the estimated truncation error on the finest grid.

Once an iteration has been completed, we can calculate several physical quantities that characterize the configuration. The total rest-mass $M_{0,\rm tot}$ is

$$M_{0,\rm tot} = \int_{\mathcal{M}} \rho_0 u^\alpha d^3\Sigma_\alpha = \int_{\mathcal{M}} \rho_0 u^t \sqrt{-g} d^3x, \qquad (59)$$

where the subscript $\mathcal{M}$ denotes integration over the support of the matter and $\sqrt{-g} = \alpha\Psi^6$. In nondimensional form we can therefore write

$$\bar{M}_{0,\rm tot} \equiv \kappa^{-n/2} M_{0,\rm tot} = \bar{r}_B^3 \int_{\mathcal{M}} \alpha\Psi^6 u^t q^n d^3\hat{x}. \qquad (60)$$

The total mass-energy (ADM mass) is

$$M_{\rm tot} = -\frac{1}{2\pi}\oint_\infty \nabla^i\Psi d^2S_i = -\frac{1}{2\pi}\int_\infty \nabla^2\Psi d^3x, \qquad (61)$$

Using the Hamiltonian constraint (44) this can be rewritten

$$M_{\rm tot} = \frac{1}{16\pi}\int_\infty \Psi^{-7}\tilde{K}_{ij}\tilde{K}^{ij} d^3x + \int_{\mathcal{M}} \Psi^5 q^n \left(\frac{1+(1+n)q}{1-v^2} - q\right) d^3x, \qquad (62)$$

or, in nondimensional form,

$$\bar{M}_{\rm tot} \equiv \kappa^{-n/2} M_{\rm tot} = \frac{\bar{r}_B}{16\pi}\int_\infty \Psi^{-7}\hat{K}_{ij}\hat{K}^{ij} d^3\hat{x} + \bar{r}_B^3 \int_{\mathcal{M}} \Psi^5 q^n \left(\frac{1+(1+n)q}{1-v^2} - q\right) d^3\hat{x}. \qquad (63)$$

Eq. (63) is the actual form we use to evaluate $M_{\rm tot}$. The angular momentum is aligned with the y-axis and can be defined as

$$J_{\rm tot} = \frac{\epsilon_{yjk}}{8\pi}\oint_\infty x^j \tilde{K}^{kl} d^2S_i = \frac{\epsilon_{yjk}}{8\pi}\int_\infty x^j \nabla_l \tilde{K}^{kl} d^3x \qquad (64)$$

(see, e.g., [32]). This is the total angular momentum contained in the spacetime and includes both the orbital and spin angular momentum of the stars. Using $\nabla_l \tilde{K}^{kl} = \Psi^{10} D_l K^{kl}$ as well as the momentum constraint (14), this can be rewritten

$$J_{\rm tot} = \int_{\mathcal{M}} \Psi^{10}(z j^x - x j^z)\, d^3x = \int_{\mathcal{M}} \Psi^{10} f_{ij}\xi^i j^j d^3x, \qquad (65)$$

where we have also used definition (23). Finally, we can substitute (42) for j^i and write the angular momentum in the nondimensional form

$$\bar{J}_{\rm tot} \equiv \kappa^{-n} J_{\rm tot} = \bar{r}_B^4 \int_{\mathcal{M}} \frac{\Psi^{10}}{\alpha} q^n \frac{1+(1+n)q}{1-v^2} f_{ij}\hat{\xi}^i(\hat{\Omega}\hat{\xi}^j - \omega^j)\, d^3\hat{x}, \qquad (66)$$

where we have rescaled $\bar{\xi}$ according to $\hat{\xi} = \bar{\xi}/\bar{r}_B$.

In the following we will denote half the total rest-mass, mass and angular momentum by $\bar{M}_0 = \bar{M}_{0,\rm tot}/2$, $\bar{M} = \bar{M}_{\rm tot}/2$ and $\bar{J} = \bar{J}_{\rm tot}/2$. In the limit of large separation, $\bar{M}_0$ and $\bar{M}$ approach the corresponding values of isolated stars.

Performing numerical simulations in three dimensions requires large computational resources. We have therefore implemented our algorithm in a parallel environment using the DAGH infrastructure [41] and run it both on the SP2 cluster at the Cornell Theory Center and the Origin2000 at the National Center for Supercomputing Applications at the University of Illinois. We typically use grids of $(64)^3$ or $(128)^3$ gridpoints, and run the code in parallel on 8 processors. DAGH has been developed as part of the Binary Black Hole Grand Challenge Project and is a package of routines and computational structures that allows for a convenient implementation of parallel applications on grid hierarchies.

B. Constructing Quasiequilibrium Sequences

In addition to constructing individual quasiequilibrium configurations, we can also build quasiequilibrium sequences of constant rest-mass $\bar{M}_0$. As we will discuss in Section V, these sequences provide approximate evolutionary tracks of inspiraling neutron star binaries.

Our quasiequilibrium configurations are parametrized by their relative separation z_A and maximum density $q_{\rm max}$. We therefore have to find a path through this two-dimensional parameter space along which $\bar{M}_0$ is constant. This can be achieved in several different ways. For example, for each separation z_A one could vary $q_{\rm max}$ until a configuration of mass $\bar{M}_0$ has been found [38]. Here we found it easier to start with a small (and hence only mildly relativistic) $q_{\rm max}$ for each z_A, and then increment $q_{\rm max}$ in small steps keeping z_A constant. The results can be tabulated, and the procedure repeated for a different z_A. Once sufficient data have been collected one can then interpolate to a chosen rest-mass $\bar{M}_0$. Note that for each $z_A = $ const sequence we adjusted the outer boundary so that the number of gridzones covering the stars is the same for all separations.

We have performed several tests to check our code. In two different regimes the results can be compared with known solutions: for small masses and weak fields we recover the Newtonian limit, and for large separations we approach the Oppenheimer-Volkoff spherical solution for each star and its near-by field. We have also checked the fully relativistic identity [42,43]

$$dM_{\rm tot} = \Omega dJ_{\rm tot}, \qquad (67)$$

which holds along constant rest-mass sequences. To evaluate Eq. (67), we have to take numerical differences between integrals of very similar magnitude, so that their relative error was much larger than that of the individual

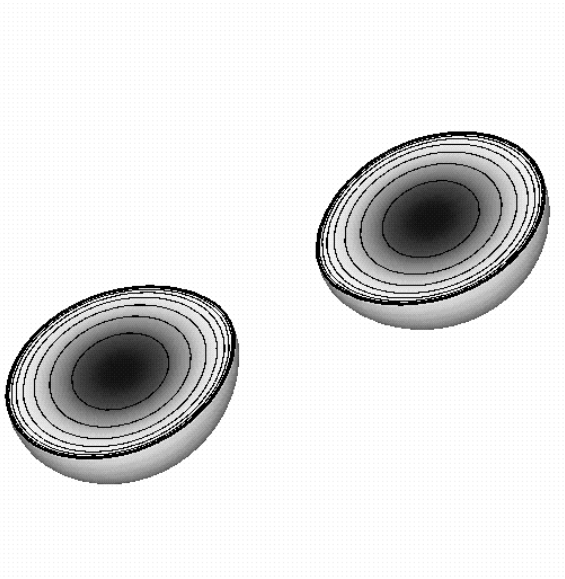

FIG. 1. Rest-density contours in the equatorial plane for a neutron star binary close to the ISCO. Each star has a rest-mass of $\bar{M}_0 = 0.169$, corresponding to a compaction in isolation of $(M/R)_\infty = 0.175$. The contours show isosurfaces of the rest-density in decreasing factors of 0.556.

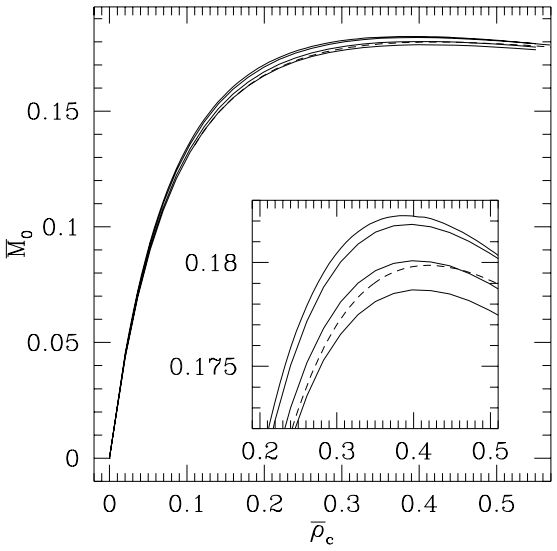

FIG. 2. Rest-Mass $\bar{M}_0$ versus maximum density $\bar{\rho}_c$ for separations $z_A = 0.3$ (bottom solid line), 0.2, 0.1 and 0.0 (top line). The dashed line is the Oppenheimer-Volkoff result for a $n = 1.0$ polytrope. The insert is a blow-up of the region around the maximum mass.

integrals. Nevertheless, we found that this identity is satisfied typically to $\sim 10\%$ (except close to turning points, where the error due to the differentiation dominates). We expect that the numerical data presented in this paper are typically accurate to within a few percent, and are confident that our code correctly predicts qualitative features, like, for example, changes in the maximum allowed mass.

V. RESULTS

A. Sequences for $n = 1.0$

In this Section we discuss configurations and sequences with a polytropic index $n = 1$, representing a fairly stiff equation of state. This is a particularly interesting example, since realistic neutron stars are expected to be governed by equations of state of similar stiffness. Results for $n = 1.5$ and $n = 2$ will be presented in Section V B. Numerical values in geometrized units can be obtained from our nondimensional "barred" quantities by multiplying with appropriate powers of κ, according to Eqs. (60), (63) and (66) (for example $M = \kappa^{n/2}\bar{M}$, $J = \kappa^n \bar{J}$, and $\rho_0 = \kappa^{-n}\bar{\rho}_0$).

In Fig. 1 we show the density profile in the equatorial plane of a binary neutron star. Here $z_A = 0.175$, and the stars are close to the ISCO (see below). Each star has a rest-mass of $\bar{M}_0 = 0.169$, corresponding to a compaction in isolation of $(M/R)_\infty = 0.175$. The contours show isosurfaces of the rest-density in decreasing factors of 0.556. The maximum compaction of a stable $n = 1.0$ polytrope in isolation is $(M/R)_\infty = 0.216$, corresponding to a maximum rest-mass $\bar{M}_0 = 0.180$ and a maximum mass $\bar{M} = 0.164$.

In Fig. 2 we plot the rest-mass $\bar{M}_0$ versus the maximum density $\bar{\rho}_c = \bar{\rho}_0^{\max} + \bar{\rho}_i^{\max}$ for several different separations between $z_A = 0.3$ (roughly two stellar radii apart) and $z_A = 0$ (touching). As $z_A \to 1$, we expect these curves to approach the spherical Oppenheimer-Volkoff (OV) result, which we included as the dashed line in Fig. 2. Note, however, that the exact OV curve is computed from a one-dimensional ordinary differential equation with very high accuracy, while the binary configurations have been calculated on very coarse, three-dimensional numerical grids. From convergence tests we know that we systematically underestimate masses, and accordingly, for large separations, we find masses slightly smaller than the corresponding OV masses. All graphs lie within less than 2% of the OV curve, showing that the presence of a companion star has only very little influence on the mass-density relationship.

As we decrease the separation, the mass supported by a given central density $\bar{\rho}_c$ increases slightly. In particular, the maximum rest-mass increases from $\bar{M}_0^{\max} = 0.179$ for $z_A = 0.3$ to $\bar{M}_0^{\max} = 0.182$ for stars in contact. This trend clearly suggests that *the maximum allowed mass of neutron stars in close binaries is slightly larger than in isolation.* This increase is caused in part by the rotation of the stars and in part by the tidal fields. More specifically, we find that the increase of the maximum al-

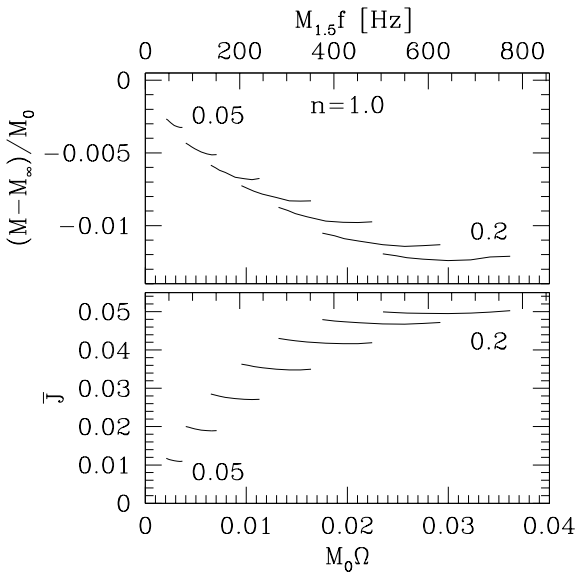

FIG. 3. Binding energy and angular momentum as a function of the angular velocity for several different values of $\bar{M}_0$. The curves are labeled by the compaction $(M/R)_\infty$ of the stars in isolation at infinity, starting with 0.05 and increasing in steps of 0.0025 up to 0.2. The maximum compaction of a stable, isolated, non-rotating $n = 1.0$ polytrope is 0.217. The upper label gives the orbital frequency for stars with a rest-mass of $1.5M_\odot$

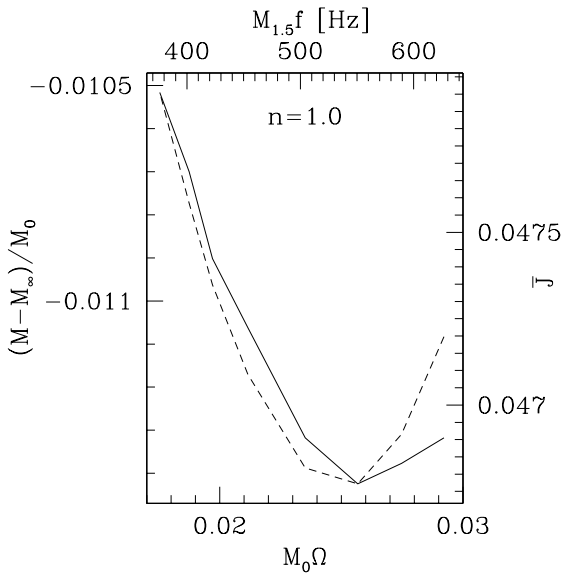

FIG. 4. Blow-up of two curves in Fig. 2: binding energy (solid) and angular momentum (dashed) as a function of the angular velocity for a binary with $\bar{M}_0 = 0.169$ and $(M/R)_\infty = 0.175$.

lowed mass is comparable to the corresponding increase of an isolated neutron star rotating with the same angular velocity [38]. Any destabilizing, relativistic effect in binaries therefore has to be smaller.

The collapse of binary neutron stars to black holes prior to merger reported by WMM could, in principle, be caused either by a decrease of the maximum allowed mass, or by a dynamical instability. As we have shown, the maximum allowed mass, within our assumptions and approximations, increases, which rules out the first possibility. Note, however, that we are only constructing quasiequilibrium configurations, which may not be dynamically stable. In [24] we show that all inspiraling binary neutron stars are *secularly* stable against radial collapse to black holes all the way down to the innermost stable circular orbit (ISCO). While this does not completely rule out the existence of a *dynamical* instability, we note that in Newtonian binaries, dynamical instabilities always occur later along equilibrium sequences than secular instabilities [44,17]. The same result has been shown for single, rotating relativistic stars [45]. Recently, Thorne [21] has argued analytically that tidal fields stabilize systems and that stars which are stable in isolation are stable with respect to both secular and dynamical modes in binary configurations.

Fig. 2 demonstrates that at fixed rest-mass, the central density decreases as the stars approach each other and get tidally deformed. This effect, as well as the increase of the maximum allowed mass, is consistent with post-Newtonian predictions [13,15,18].

Next we construct sequences of constant rest-mass $\bar{M}_0$, which up to the ISCO approximate evolutionary sequences. As discussed in Section II, we maintain corotation, whereas in reality it is more likely that circulation will be conserved. Nevertheless, our sequences are the first sequences of inspiraling binaries in full general relativity. Moreover, post-Newtonian sequences of constant circulation are not vastly different from corotating sequences [15]. In Fig. 3 we plot the binding energy $(M - M_\infty)/M_0$ and the angular momentum $\bar{J}$ as a function of separation for several different rest-masses. Since the separation is not an invariant quantity, we have parametrized the sequence by the nondimensionalized angular velocity $M_0\Omega$ $(= \bar{M}_0\bar{\Omega})$. Our curves do not connect to $M_0\Omega = 0$, corresponding to infinite separation, since we can numerically resolve only fairly close models.

In the top half of Fig. 3 we show plots for sequences for several different, increasingly relativistic rest-masses. The curves are labeled by the compaction $(M/R)_\infty$ that the stars would have in isolation at infinity. We have plotted graphs for $(M/R)_\infty$ between 0.05 and 0.2 in increments of 0.025. In the lower half of Fig. 3 we show corresponding plots of $\bar{J}$. According to Eq. (67) the minima in both curves must agree, which they do within our numerical accuracy. In Fig. 4 we show a blow-up of the two curves for stars with $(M/R)_\infty = 0.175$.

For infinitely separated stars, both the binding energy and the angular velocity vanish. As the stars approach

$\bar{M}_0$	$\bar{M}_\infty$	$(M/R)_\infty$	$M_0\Omega_{ISCO}$	$(J_{\rm tot}/M^2_{\rm tot})_{ISCO}$
0.059	0.058	0.05	0.003	1.69
0.087	0.084	0.075	0.0065	1.37
0.112	0.106	0.1	0.01	1.22
0.134	0.126	0.125	0.015	1.12
0.153	0.142	0.15	0.02	1.05
0.169	0.155	0.175	0.025	1.00
0.178	0.162	0.2	0.03	0.97

TABLE II. Numerical values for sequences of constant rest-mass $\bar{M}_0$ and polytropic index $n = 1$. We tabulate the total energy $\bar{M}_\infty$ and compaction $(M/R)_\infty$ each star would have in isolation as well as the angular velocity $M_0\Omega$ and the angular momentum $J_{\rm tot}/M^2_{\rm tot}$ at the ISCO. The maximum rest-mass in isolation is $\bar{M}_0^{\rm max} = 0.180$.

each other, the angular velocity increases while the binding energy decreases. This effect is essentially Newtonian and is even evident for two Newtonian point masses. As the stars approach, however, finite size effects eventually play an important role. The energy associated with the rotation of the individual stars adds to the (negative) binding energy, and therefore reduces it. For stiff enough equations of state, for which the moment of inertia and hence the rotational energy of the individual stars is large (see Section V B), the binding energy goes through a minimum and then increases again prior to contact. The location of the minimum marks the onset of a secular instability, beyond which the binary can no longer maintain corotation. It is expected that the dynamical instability defining the ISCO occurs after, but close to the onset of the secular instability [44,17]. In the following we will refer to the location of the minimum as the ISCO.

The upper labels give the orbital frequency in Hz for stars of rest-mass $1.5M_\odot$. The corresponding gravitational wave frequency is larger by a factor of 2 for the dominant quadrupole mode. For small values of the compaction we find ISCO frequencies comparable to those reported by WMM. However, for larger compaction and more relativistic configurations we find frequencies very similar to what is found from post-Newtonian calculations [46].

We summarize our results in Table 2, where we also include the dimensionless angular momentum $J_{\rm tot}/M^2_{\rm tot} = J/2M^2$ at the ISCO. For small rest-masses, this value is larger than unity, in agreement with WMM. For high enough rest-masses, however, it drops below unity, so that the two stars could plunge and form a Kerr black hole without having to lose additional angular momentum.

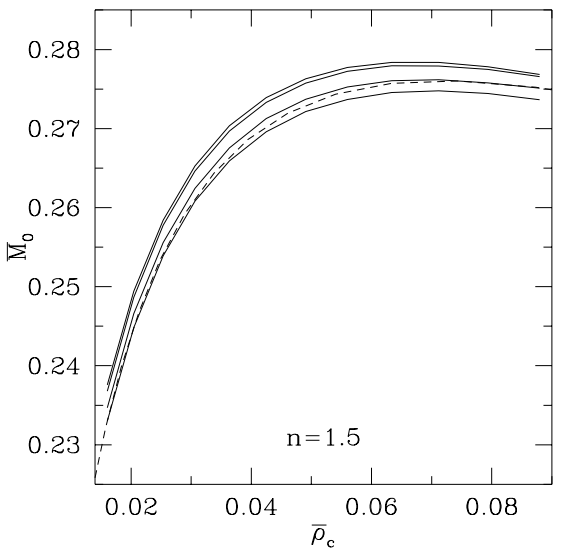

FIG. 5. Rest-Mass $\bar{M}_0$ of a $n = 1.5$ polytrope versus maximum density $\bar{\rho}_c$ for separations $z_A = 0.3$ (bottom solid line), 0.2, 0.1 and 0.0 (top line). The dashed line is the Oppenheimer-Volkoff result.

B. Sequences for $n = 1.5$ and $n = 2.0$

In this Section we will present results for polytropic indices of $n = 1.5$ and 2.0, representing softer equations of state. Except for the absence of an ISCO prior to contact (see below) all results are qualitatively very similar to those for $n = 1$. In particular, we consistently find a decrease of the maximum density as the stars approach, and an increase in the maximum allowed mass. The relative size of these effects differs for three basic reasons: First, for softer equations of state, the maximum mass of a star occurs at a smaller value of the compaction M/R, and hence relativistic effects play a smaller role. Second, for softer equations of state these stars are more centrally condensed. We therefore expect tidal fields to play a less important role for the stability of these stars in close binaries. While it is easier to deform their surface, the bulk of the matter is very concentrated at the core of the stars and well shielded from the tidal field of the companion. Third, for softer equations of state, the stars have a smaller orbital frequency even at very small separations, so that the effects of rotation are smaller. Accordingly we find that the maximum allowed mass still increases with decreasing separation, but the effect is smaller than for $n = 1$.

More centrally condensed stars have a smaller moment of inertia, and hence the rotational kinetic energy associated with the spin of the stars is smaller than for less centrally condensed stars. Therefore a turning point in the binding energy curve can only be expected for stars with a stiff enough equation of state. This effect has been

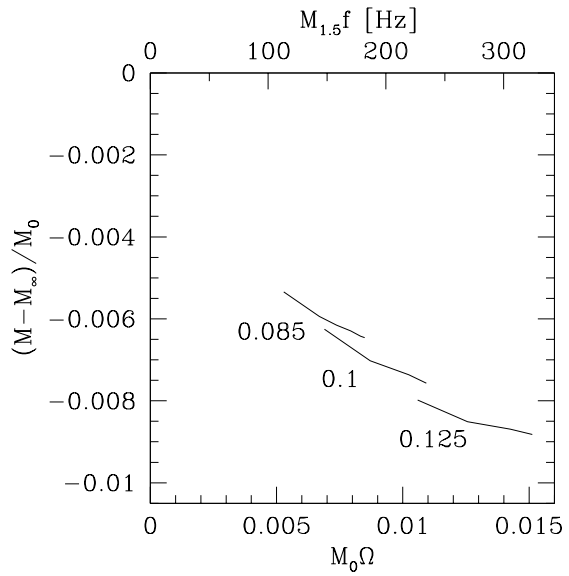

FIG. 6. Binding energy of $n = 1.5$ polytropes as a function of the angular velocity for different rest-masses. The curves are labeled by the compaction $(M/R)_\infty$ of the stars in isolation. The maximum compaction for a stable, isolated, nonrotating $n = 1.5$ polytrope is 0.136.

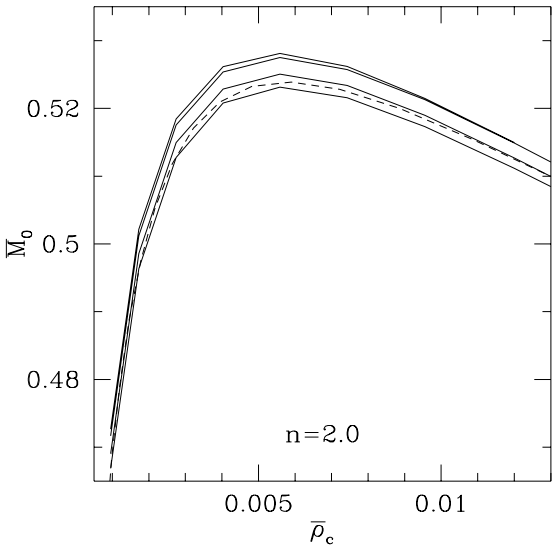

FIG. 7. Same as Fig. 5 for a $n = 2.0$ polytrope.

discussed by several authors in the context of Newtonian theory [47,17,48]. We did not see a turning point for $n \geq 1.5$, in agreement with [47,48]. For these polytropic indices there is no ISCO prior to contact, and we expect the orbits to be stable until the stars touch and form a contact binary. This is the first construction of a contact binary in full general relativity. Proving the existence of a contact binary neutron star (by, e.g., the signature of its gravitational waveform) would indicate that the equation of state of nuclear matter is rather soft. We do not expect this to be the case [49].

In Fig. 5 we plot the rest-mass versus the central density for several different separations for $n = 1.5$. Qualitatively the result is very similar to Fig. 2 for $n = 1$: For all separations the curve differs from the OV result by less than 1%. For decreasing separation we find a small increase in the allowed mass that a given density can support. In particular, the maximum quasiequilibrium rest-mass increases by roughly 1.2% from $\bar{M} = 0.275$ for $z_A = 0.3$ to 0.278 for stars in contact. For $n = 1$ the corresponding increase is about 2 %. The maximum density decreases as the stars approach and get tidally deformed.

In Fig. 6 we plot the binding energy of $n = 1.5$ polytropes as a function of the angular velocity. We show results for several different rest-masses and label them by the compaction $(M/R)_\infty$ for the same stars in isolation. In contrast to the results for $n = 1$, these curves no longer show a turning point. This implies that the stars are secularly stable all the way to touching.

In Figs. 7 and 8 we show the corresponding results for $n = 2$ polytropes. Again, in Fig. 7 we show the rest-mass

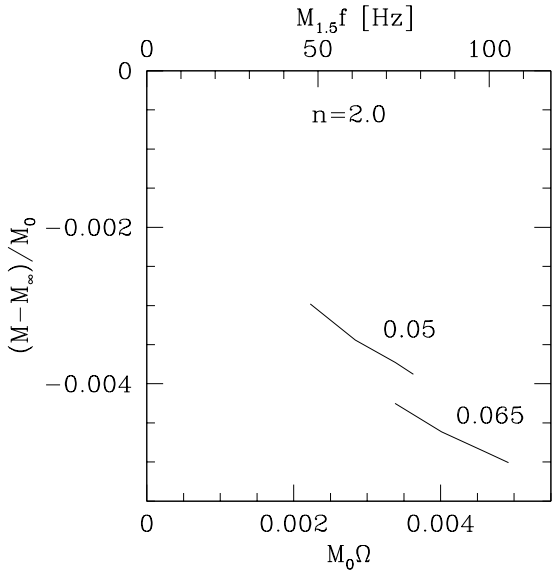

FIG. 8. Same as Fig. 6 for a $n = 2.0$ polytrope. The maximum compaction $(M/R)_\infty$ for a stable, isolated, nonrotating $n = 1.5$ polytrope is 0.075.

versus central density. The maximum quasiequilibrium rest-mass increases from $\bar{M} = 0.523$ for $z_A = 0.3$ to 0.528 for touching stars. This relative increase of roughly 1 % is smaller than even for $n = 1.5$. As expected, the binding energies in Fig. 8 do not show a turning point, so that the binaries are secularly stable all the way to touching.

VI. SUMMARY AND CONCLUSIONS

We report on the first fully relativistic calculation of binary neutron stars in quasiequilibrium. We previously presented some of our preliminary results in [23]; here we describe in detail all our assumptions and approximations, equations and numerical algorithm, as well as results for different polytropic indices. We integrate a subset of Einstein's equations, coupled to the equation of hydrostatic equilibrium, to solve the initial value problem for binaries. We construct models of corotating binary neutron stars in close circular orbit, including relativistic models of contact binaries. We also construct sequences of constant rest-mass configurations parametrized by their separation and orbital angular frequency.

We find that the maximum density of the stars decreases as the stars approach and get tidally deformed. Simultaneously, the mass that a given maximum density can support increases as the stars approach. In particular, we find that the maximum allowed mass of neutron stars in quasiequilibrium binaries increases with decreasing separation. These effects are larger for smaller polytropic index (and hence stiffer equation of state).

Searching for turning points of the binding energy of constant rest mass sequences, we locate, for small enough polytropic index, the ISCO. As in the case of Newtonian configurations, an ISCO exists only for indices $n \lesssim 1.5$; for softer equations of state, contact is reached prior to the onset of orbital instability.

In [24] we presented a more careful analysis of the radial stability of relativistic binary neutron stars against collapse. We showed that all inspiraling binary neutron stars are secularly stable against radial collapse to black holes all the way to the ISCO (or contact, if, for large enough n, no ISCO is encountered). We do not find any evidence for a destabilization of neutron stars in close binary orbits.

ACKNOWLEDGMENTS

It is a pleasure to thank Manish Parashar for his help with the implementation of DAGH, and Andrew Abrahams, James Lombardi and Fred Rasio for several helpful discussions. We would also like to thank Matthew Duez, Eric Engelhard and John Fregeau for helping with the visualization of our data and the production of Fig. 1. This work was supported by NSF Grant AST 96-18524 and NASA Grant NAG 5-3420 at Illinois, NSF Grant PHY 94-08378 at Cornell, and by the NSF Binary Black Hole Grand Challenge Grant Nos. NSF PHY 93-18152/ASC 93-18152 (ARPA supplemented). Computations were performed at the Cornell Center for Theory and Simulation in Science and Engineering and the National Center for Supercomputing Applications, University of Illinois at Urbana-Champaign.

[1] S. E. Thorsett, Z. Arzoumanian, M. M. McKinnon and J. H. Taylor, Astrophys. J. **405**, L29 (1993)
[2] J. H. Taylor and J. M. Weisberg, Astrophys. J. **345**, 434 (1989)
[3] Z. Arzoumanian, PhD thesis, Princeton University (1995)
[4] I. Hachisu and Y. Eriguchi, Publ. Astron. Soc. Japan **36**, 239 (1984)
[5] F. A. Rasio and S. L. Shapiro, Astrophys. J. **401**, 226 (1992); **432**, 242 (1994)
[6] M. Shibata, T. Nakamura and K. Oohara, Prog. Theor. Phys. **88**, 1079 (1992)
[7] X. Zhuge, J. M. Centrella and S. L. W. McMillan, Phys. Rev. D **50**, 6247 (1994); **54**, 7261 (1996);
[8] M. Ruffert, H.-T. Janka and G. Schäfer, Astrophys. Sp. Sci. **231**, 423 (1995)
[9] L. Blanchet, T. Damour, B. R. Iyer, C. M. Will and A. G. Wiseman, Phys. Rev. Lett. **74**, 3515 (1995) and references therein
[10] M. Shibata, Prog. Theor. Phys. **96**, 317 (1996); Phys. Rev. D. **55**, 6019 (1997)
[11] K. Taniguchi and M. Shibata, 1997, to appear in Phys. Rev. D. (gr-qc/9705027); M. Shibata and K. Taniguchi, 1997, to appear in Phys. Rev. D. (gr-qc/9705028)
[12] K. Oohara and T. Nakamura, Lecture delivered at Les Houches School "Astrophysical Sources of Gravitational Radiation" (Les Houches, France, Sept. 26 - Oct. 6, 1995). To be published in the Proceedings (eds. J.-A. Marck and J.-P. Lasota) (astro-ph/9606179)
[13] D. Lai, Phys. Rev. Lett. **76**, 4878 (1996)
[14] D. Lai and A. D. Wiseman, Phys. Rev. D **54**, 3958 (1996)
[15] J. C. Lombardi, F. A. Rasio and S. L. Shapiro, 1997, Phys. Rev. D, in press (astro-ph/9705218)
[16] J. R. Wilson and G. J. Mathews, Phys. Rev. Lett. **75**, 4161 (1995); J. R. Wilson, G. J. Mathews and P. Marronetti, Phys. Rev. D **54**, 1317 (1996) (WMM)
[17] D. Lai, F. A. Rasio and S. L. Shapiro, Astrophys. J. Suppl. 88, 205 (1993)
[18] A. D. Wiseman, Phys. Rev. Lett. **79**, 1189 (1997)
[19] P. R. Brady and S. A. Hughes, Phys. Rev. Lett. **79**, 1186 (1997)
[20] É. É. Flanagan, 1997, submitted (gr-qc/9706045)
[21] K. S. Thorne, 1997, submitted (gr-qc/9706057)
[22] D. M. Eardley and E. W. Hirschmann, preprint NSF-ITP-95-165 (1995) (astro-ph/9601019)
[23] T. W. Baumgarte, G. B. Cook, M. A. Scheel, S. L.

Shapiro and S. A. Teukolsky, Phys. Rev. Lett. **79**, 1182 (1997)
[24] T. W. Baumgarte, G. B. Cook, M. A. Scheel, S. L. Shapiro and S. A. Teukolsky, 1997, submitted (gr-qc/9705023)
[25] L. Bildsten and C. Cutler, Astrophys. J. **400**, 175 (1992)
[26] C. S. Kochanek, Astrophys. J. **398**, 234 (1992)
[27] J. R. Wilson and G. J. Mathews, in *Frontiers in Numerical Relativity*, edited by C. R. Evans, L. S. Finn, and D. W. Hobill (Cambridge University Press, Cambridge, England, 1989), pp. 306;
[28] G. B. Cook, S. L. Shapiro and S. A.Teukolsky, Phys. Rev. D **53**, 5533 (1996)
[29] R. Arnowitt, S. Deser and C. W. Misner, in *Gravitation*, edited by L. Witten (Wiley, New York, 1962)
[30] J. W. York, Jr., Phys. Rev. Lett. **28**, 1082 (1972); Niall Ó Murchadha and J. W. York, Jr., Phys. Rev. D, **10**, 428 (1974)
[31] Note that we could have chosen any metric for which $\gamma^{-1/3}\gamma_{ij}$ is independent of time. Choosing a conformally flat metric leads to familiar flat-space differential operators.
[32] J. M. Bowen and J. W. York, Jr., Phys. Rev. D **21**, 2047 (1980)
[33] J. M. Bowen, Gen. Rel. Grav. **14**, 1183 (1982)
[34] A. P. Lightman, W. H. Press, R. H. Price and S. A. Teukolsky, *Problem Book in Relativity and Gravitation* (Princeton University Press, Princeton, New Jersey, 1975), problem 16.17
[35] We will loosely refer to q as the density, even though the density is really $\kappa^{-n}q^n$.
[36] I. Hachisu, Astrophys. J. Suppl. **61**, 479 (1986)
[37] H. Komatsu, Y. Eriguchi and I. Hachisu, Mon. Not. R. Astron. Soc. **237**, 355 (1989)
[38] G. B. Cook, S. L. Shapiro and S. A.Teukolsky, Astrophys. J. **398**, 203 (1992); Astrophys. J. **422**, 227 (1994)
[39] W. H. Press, S. A. Teukolsky, W. T. Vetterling and B. P.Flannery, *Numerical Recipes in Fortran, Second Edition* (Cambridge University Press, Cambridge, 1992)
[40] Note that we limit this search to the z-axis, whereas in general the maximum density may occur elsewhere inside the star. However, this is not a limitation of our method and also we have found that in all our simulations the maximum density did indeed occur on the z-axis.
[41] M. Parashar and J. C. Brown, in *Proceedings of the International Conference for High Performance Computing*, eds. S. Sahni, V. K. Prasanna and V. P. Bhatkar (Tata McGraw-Hill Publishing Company Ltd, 1995), also `www.ticam.utexas.edu/~parashar/public_html/DAGH/`
[42] J. B. Hartle, Astrophys. J. **161**, 111 (1970)
[43] J. M. Bardeen, in *Black Holes*, ed. C. DeWitt (New York: Gordon & Breach, 1972)
[44] S. Chandrasekhar, Astrophys. J. **161**, 561 (1970)
[45] J. L. Friedman, J. R. Ipser and R. D. Sorkin, Astrophys. J. **325**, 722 (1988)
[46] L. E. Kidder, C. M. Will and A. G. Wiseman, Phys. Rev. D **47**, 3281 (1993)
[47] I. Hachisu, Astrophys. J. Suppl. **62**, 461 (1986)
[48] F. A. Rasio and S. L. Shapiro, Astrophys. J. **432**, 242 (1994)
[49] S. L. Shapiro and S. A. Teukolsky, *Black Holes, White Dwarfs, and Neutron Stars* (New York, Wiley, 1983)

APPENDIX A: NUMERICAL RESULTS FOR SELECTED SEQUENCES

In the following we tabulate numerical values for selected sequences. For a given polytropic index n and the rest-mass (baryon mass) $\bar{M}_0$ of one star (or equivalently its compaction in isolation $(M/R)_\infty$), we list the relative separation $z_A = \bar{r}_A/\bar{r}_B$, the maximal density parameter $q^{\max}$, the mass $\bar{M}$ the angular momentum $\bar{J}$, the (orbital) frequency $\bar{\Omega}$, and the locations $\bar{r}_A$, $\bar{r}_B$ and $\bar{r}_C$. We have "barred" these quantities as a reminder that they are dimensionless coordinate values. Recall that ρ, ρ_0 and P may be obtained from q via Eqs. (37) – (39).

$n = 1$, $\bar{M}_0 = 0.0595$, $(M/R)_\infty = 0.05$

z_A	$q^{\max}$	$\bar{M}$	$\bar{J}$	$\bar{\Omega}$	$\bar{r}_A$	$\bar{r}_B$	$\bar{r}_C$
0.00	0.0275	0.057806	0.01095	0.061	0.000	1.529	2.773
0.10	0.0278	0.057806	0.01094	0.057	0.281	1.594	2.810
0.15	0.0281	0.057809	0.01098	0.053	0.430	1.677	2.868
0.20	0.0284	0.057815	0.01109	0.048	0.591	1.791	2.959
0.25	0.0286	0.057825	0.01129	0.042	0.771	1.940	3.087
0.30	0.0288	0.057836	0.01155	0.037	0.975	2.118	3.251

TABLE III.

$n = 1$, $\bar{M}_0 = 0.1118$, $(M/R)_\infty = 0.1$

z_A	$q^{\max}$	$\bar{M}$	$\bar{J}$	$\bar{\Omega}$	$\bar{r}_A$	$\bar{r}_B$	$\bar{r}_C$
0.00	0.0658	0.105511	0.02715	0.101	0.000	1.289	2.353
0.10	0.0667	0.105502	0.02707	0.094	0.238	1.346	2.384
0.15	0.0676	0.105509	0.02710	0.087	0.365	1.418	2.433
0.20	0.0685	0.105521	0.02729	0.079	0.502	1.516	2.511
0.25	0.0693	0.105558	0.02766	0.070	0.655	1.644	2.621
0.30	0.0698	0.105593	0.02818	0.062	0.828	1.797	2.763

TABLE IV.

$n = 1$, $\bar{M}_0 = 0.1341$, $(M/R)_\infty = 0.125$

z_A	$q^{\max}$	$\bar{M}$	$\bar{J}$	$\bar{\Omega}$	$\bar{r}_A$	$\bar{r}_B$	$\bar{r}_C$
0.00	0.0912	0.124786	0.03496	0.122	0.000	1.172	2.148
0.10	0.0926	0.124785	0.03482	0.114	0.217	1.225	2.175
0.15	0.0940	0.124787	0.03482	0.106	0.332	1.291	2.219
0.20	0.0954	0.124819	0.03500	0.096	0.458	1.381	2.290
0.25	0.0967	0.124849	0.03538	0.086	0.597	1.498	2.390
0.30	0.0976	0.124898	0.03596	0.076	0.756	1.639	2.520

TABLE V.

$n = 1$, $\bar{M}_0 = 0.1534$, $(M/R)_\infty = 0.15$

z_A	$q^{\max}$	$\bar{M}$	$\bar{J}$	$\bar{\Omega}$	$\bar{r}_A$	$\bar{r}_B$	$\bar{r}_C$
0.00	0.1235	0.140851	0.04188	0.146	0.000	1.056	1.943
0.10	0.1256	0.140842	0.04167	0.137	0.196	1.104	1.967
0.15	0.1280	0.140846	0.04162	0.127	0.300	1.163	2.005
0.20	0.1303	0.140859	0.04174	0.116	0.413	1.244	2.067
0.25	0.1325	0.140903	0.04210	0.104	0.539	1.350	2.156
0.30	0.1341	0.140971	0.04268	0.092	0.682	1.477	2.273

TABLE VI.

$n = 1$, $\bar{M}_0 = 0.1685$, $(M/R)_\infty = 0.175$

z_A	$q^{\max}$	$\bar{M}$	$\bar{J}$	$\bar{\Omega}$	$\bar{r}_A$	$\bar{r}_B$	$\bar{r}_C$
0.00	0.1647	0.152893	0.04719	0.173	0.000	0.944	1.743
0.10	0.1683	0.152883	0.04691	0.163	0.176	0.987	1.762
0.15	0.1726	0.152875	0.04677	0.152	0.268	1.038	1.792
0.20	0.1769	0.152893	0.04681	0.139	0.368	1.108	1.844
0.25	0.1811	0.152936	0.04708	0.125	0.480	1.201	1.920
0.30	0.1844	0.152997	0.04758	0.111	0.606	1.312	2.022

TABLE VII.

$n = 1$, $\bar{M}_0 = 0.1781$, $(M/R)_\infty = 0.2$

z_A	$q^{\max}$	$\bar{M}$	$\bar{J}$	$\bar{\Omega}$	$\bar{r}_A$	$\bar{r}_B$	$\bar{r}_C$
0.00	0.2164	0.160183	0.05024	0.202	0.000	0.841	1.560
0.10	0.2228	0.160174	0.04989	0.191	0.157	0.877	1.572
0.15	0.2327	0.160137	0.04963	0.180	0.238	0.917	1.587
0.20	0.2450	0.160130	0.04948	0.168	0.323	0.970	1.616
0.25	0.2590	0.160145	0.04953	0.154	0.415	1.038	1.662
0.30	0.2741	0.160189	0.04975	0.139	0.517	1.119	1.725

TABLE VIII.

$n = 1.5$, $\bar{M}_0 = 0.241$, $(M/R)_\infty = 0.85$

z_A	$q^{\max}$	$\bar{M}$	$\bar{J}$	$\bar{\Omega}$	$\bar{r}_A$	$\bar{r}_B$	$\bar{r}_C$
0.00	0.0626	0.231583	0.13408	0.035	0.000	3.409	6.227
0.10	0.0633	0.231623	0.13471	0.032	0.631	3.569	6.318
0.20	0.0650	0.231708	0.13738	0.027	1.328	4.014	6.642
0.30	0.0665	0.231853	0.14341	0.021	2.184	4.740	7.281

TABLE IX.

$n = 1.5$, $\bar{M}_0 = 0.258$, $(M/R)_\infty = 0.1$

z_A	$q^{\max}$	$\bar{M}$	$\bar{J}$	$\bar{\Omega}$	$\bar{r}_A$	$\bar{r}_B$	$\bar{r}_C$
0.00	0.0794	0.246547	0.14275	0.042	0.000	3.038	5.561
0.10	0.0802	0.246600	0.14346	0.039	0.564	3.183	5.643
0.20	0.0831	0.246688	0.14574	0.033	1.180	3.564	5.902
0.30	0.0855	0.246887	0.15166	0.026	1.938	4.204	6.460

TABLE X.

$n = 1.5$, $\bar{M}_0 = 0.2745$, $(M/R)_\infty = 0.125$

z_A	$q^{\max}$	$\bar{M}$	$\bar{J}$	$\bar{\Omega}$	$\bar{r}_A$	$\bar{r}_B$	$\bar{r}_C$
0.00	0.1119	0.260578	0.14820	0.055	0.000	2.549	4.680
0.10	0.1141	0.260614	0.14830	0.051	0.472	2.658	4.722
0.20	0.1237	0.260665	0.14908	0.045	0.964	2.909	4.824
0.30	0.1380	0.260810	0.15227	0.038	1.518	3.291	5.061

TABLE XI.

$n = 2$, $\bar{M}_0 = 0.495$, $(M/R)_\infty = 0.05$

z_A	$q^{\max}$	$\bar{M}$	$\bar{J}$	$\bar{\Omega}$	$\bar{r}_A$	$\bar{r}_B$	$\bar{r}_C$
0.00	0.0381	0.48628	0.7204	0.0073	0.000	12.89	23.47
0.10	0.0383	0.48635	0.7281	0.0068	2.382	13.49	23.82
0.20	0.0389	0.48649	0.7508	0.0057	4.998	15.11	24.99
0.30	0.0395	0.48672	0.7924	0.0045	8.192	17.78	27.30

TABLE XII.

$n = 2$, $\bar{M}_0 = 0.52$, $(M/R)_\infty = 0.065$

z_A	$q^{\max}$	$\bar{M}$	$\bar{J}$	$\bar{\Omega}$	$\bar{r}_A$	$\bar{r}_B$	$\bar{r}_C$
0.00	0.0493	0.50929	0.7190	0.0095	0.000	10.70	19.52
0.10	0.0497	0.50936	0.7255	0.0089	1.976	11.18	19.76
0.20	0.0525	0.50950	0.7409	0.0077	4.069	12.30	20.34
0.30	0.0574	0.50969	0.7679	0.0065	6.432	13.95	21.44

TABLE XIII.